June 4, 1999 3:34 pm

Ice Flow in the North East Greenland Ice Stream

Ian Joughin,
Jet Propulsion Laboratory, California Institute of Technology
M/S 300-235, 4800 Oak Grove Drive, Pasadena, CA 91109, USA
Ph: 818-354-1587 Fax: 818-393-3077 Email; Ian@radar-sci.jpl.nasa.gov

Mark Fahnestock
Earth System Science Interdisciplinary Center, University of Maryland
College Park, MD 20742, USA

Jonathan L. Bamber
Centre for Remote Sensing, School of Geographical Sciences, University of Bristol,
University Road,
Bristol, BS8 1SS, UK.

Doug MacAyeal,
Dept. of Geophysical Sciences, Univ. of Chicago
5734 S. Ellis Ave., Chicago, IL 60637, USA

We have measured ice flow and detailed topography in northeastern Greenland using satellite-based Synthetic Aperture Radar (SAR) interferometry. The object of this study is the large ice stream that drains this quadrant of the ice sheet. A single SAR interferogram allows the measurement of one component of motion over a several-day long interval. We have used a set of such measurements, from several look directions, to produce a mosaic of ice flow velocity. The resulting flow field is tied to an estimated balance velocity distribution in slow moving areas, and assumes flow to be locally surface parallel. In spite of these assumptions, the velocity field is the most detailed, consistent data set available over a flow feature of this size. It compares with GPS control points at the 5 m/yr level. In the process of mapping ice flow velocity, an enhanced elevation model of the ice stream was produced. The elevation model is based on a blend of interferometrically-derived short wavelength topography and radar-altimetry based longer wavelength topography. This enhanced model has improved information on local surface slope, which was useful for estimating the horizontal components of the velocity field.

Specific Topics: Ice Streams, Ice Sheets, Remote Sensing

Introduction

The remoteness and harsh environments of Greenland and Antarctica make *in situ* collection of ice velocity and elevation data difficult. The field measurements that have been made have come at great expense and human effort. Over the last decade, satellite remote sensing has reached a point where it is now possible to make accurate, high-resolution measurements of many ice sheet parameters. Radar altimeters, for example, have provided elevation models over all of Greenland and much of Antarctica (Bamber and Others, 1997). Recently introduced (Goldstein and others, 1993), satellite radar interferometry has emerged as a powerful method for measuring ice-flow velocity and surface topography.

Spaceborne observations are, for the most part, limited to the surface of the ice sheet. Yet many of the controls on ice flow manifest themselves below the surface. Inversions of ice sheet models constrained by remotely sensed data have been used to help understand internal dynamical processes of ice flow (MacAyeal and others, 1995). While yielding promising results, the development and further application of such inverse techniques has been limited by a scarcity of data. Satellite radar interferometry now provides a means to begin filling this data gap.

We have begun an investigation that uses a combination of remote sensing and modeling techniques to study the northeast Greenland ice stream. This ice stream was first recognized in satellite imagery, where it appears as a nearly straight feature about 700 km long, with identifiable margins for most of its length and a topographically undulating interior due to the rapid ice flow (Fahnestock and others. 1993). The organized flow extends far into the interior, beginning within about 100 km of the ice divide. Nearer the coast it has low-slope areas of rapid flow and regions of enhanced shear that resemble the ice streams of West Antarctica.

This paper describes the remote sensing component of our investigation. We present a vector velocity map that covers the entire ice stream. We describe the map generation and validate our results through a comparison with independent GPS measurements. Finally, we describe the use of interferometric techniques to improve the resolution of a Digital Elevation Model (DEM) for the ice stream that was originally derived primarily from radar altimetry data.

Velocity Field

Fig. 1 shows the final product, a velocity map, that we have derived for the northeast Greenland ice stream, using interferometric data from several ascending and descending ERS orbits. These data were collected during the ice and commissioning orbital phases of ERS-1 as well as the ERS-1 and 2 tandem mission.

The velocity map confirms that the ice stream begins as a narrow (10-15 km) tributary of enhanced flow. Although the flow is not exceptionally fast at this point (e.g. 15-30 m/yr), its speed is well above that of the surrounding ice with well defined shear margins (see profile A in Fig 1). Further down stream a second tributary of enhanced flow merges with the ice stream. This tributary is much broader and, in contrast to the first tributary, lacks well defined shear margins (see profile B in Fig 1).

Roughly 100 km downstream, the ice stream broadens out to a width of nearly 50 kilometers with speeds of 50-75 m/yr (profile C in Fig 1.). From here, the speed increases gradually downstream over the next 200 kilometers until the ice undergoes an abrupt change in speed from around 100 m/yr to 300-400 m/yr over a distance of around 20 kilometers (profile D). This increase in speed is coincident with a peak and then rapid decline in the driving stress, which is similar in character to that observed for ice stream onsets in West Antarctica (Bentley, 1987). The flow then divides to contribute ice to three major outlet glaciers: Nioghalvfjerdsbrae, Zachariae, and Storstrømmen. The data also show that Nioghalvfjerdsbrae derives a large part of its ice from an independent tributary.

Control Points

Interferometric estimates of ice velocity require cm-level accuracies for the interferometer baseline (Joughin and Others, 1996b). Baselines determined from precision state vectors generally do not provide sufficient accuracy for most glaciological applications. Instead, elevation and velocity control points are needed to solve for the baseline.

For regions near the coast, areas of exposed bedrock can be used for control, eliminating the need for velocity measurements (Joughin and Others, 1996b). Many of the scenes we used, however, were well away from the coast so that there was with little or no ice free area to provide control.

We had originally intended to use GPS surveyed velocities as control points, which were collected by the National Aeronautics and Space Administration (NASA) Program for Arctic Regional Climate Assessment (PARCA) along the 2000-meter contour of Greenland to measure ice sheet outflow (R. Thomas, unpublished data). Additional data were collected as part of this effort near the onset area of the ice stream specifically for use as interferometric control points. The points used in our study are indicated in Fig. 1 with red + symbols. Unfortunately, there was an insufficient number of points to provide control for all of the interferometric swaths. Furthermore, in swaths where we did have at least the minimum of four points available, interferometric phase errors were often so large as to prevent us from achieving the desired baseline accuracy. Because we use a least-squares fit to the control points to determine the baseline parameters, it is possible to mitigate the effects of phase noise by using a larger number of

control points. We did not, however, have the resources to collect these data.

With an insufficient number of GPS control points, we opted to use balance velocities as a source of control. Balance velocities are the depth-averaged velocities necessary to maintain the steady-state shape of the ice sheet and are estimated from surface slope, ice thickness, and accumulation data (Paterson, 1994). We computed these values as described by Joughin and Others (1997) and rescaled them by a factor of 1.1 to obtain surface velocity estimates.

Errors in the source data (e.g., accumulation, thickness) can lead to large errors in the balance-velocity estimates. In addition, since estimates represent the velocity field averaged over 10-20 ice thickness, the estimates have inherently low resolution. To minimize the impact of balance-velocity errors on our baseline estimates, we selected control points in slow-moving areas outside of the ice stream, where the absolute errors in the balance velocities are small. For example, if the velocity is 10 m/yr, then even a large relative error of 50 percent error leads to an absolute error of only 5 m/yr.

To keep absolute errors small, we used only control points where the balance velocity was less than 40 m/yr. There are 26 GPS points from the area shown in Figure 1 that meet this criteria, allowing us to quantify the balance velocity error. If we assume zero error in the GPS estimates, then the Root Mean Squared (RMS) error is given by,

$$\text{RMS ERROR} = \sqrt{mean((v_{b,x} - v_{GPS,x})^2 + (v_{b,y} - v_{GPS,y})^2)}, \qquad (1)$$

where the x and y directions are defined by the polar stereographic projection (x directed south along -45 deg longitude, y along -135 deg). Using this metric, the error for the 26 points is 5.5 m/yr. For many of the interior strips, we were able to set a much lower threshold for the balance velocities. For an upper limit of 10 m/yr, the RMS error drops to 2.4 m/yr for the 12 GPS points that lie below this threshold.

The comparison with GPS data indicates that the balance velocities provide a reasonable source of control. With the ability to use several dozen points in each baseline solution, we are able to greatly reduce the effects of interferometric phase noise on the baseline solution. In addition, the large number of points helps mitigate the effect of the random component of the control-point noise. This does little, however, to reduce the effect of systematic trends in the control-point data (i.e., a linear error in the balance velocities across a scene).

Baseline estimates need the elevation at the control points. On the ice, the elevation control data we used were extracted from a DEM derived primarily from radar altimetry (Bamber and others, 1997). Additional data from ice free areas were derived from a DEM produced by the Danish National Survey and Cadastre (Ekholm, 1996).

Velocity Map Generation

To create our map, we began by solving for the baseline for each individual swath. For the ascending swaths we relied entirely on balance velocities and ice free points near the coast. For the descending data we first determined the baselines for the inland descending swaths using balance velocities. We then produced a map of velocity for the inland areas. Next, we used data from the faster moving points of this initial map to provide a source of control for the descending swaths nearer the coast. By bootstrapping in this manner, we were able to avoid the direct use of balance velocities for some of the swaths with predominately fast motion.

The technique we used to make velocity measurements for individual scenes has been described elsewhere (Joughin and Others, 1996b,1998). Unlike earlier maps that we have produced, this map involved combining many swaths of crossing ascending and descending orbits (17 swaths of data). The intersections of pairs of crossing orbits produce a small patches that must be mosaicked together to create the overall map. The number of these small patches is generally much larger than the number of SAR swaths.

In the mosaicking process for each ascending image, we looped through the descending images to find the areas of overlap over which to estimate the velocity. To avoid discontinuities, we weighted the edges of each patch with a linear taper. While this "feathering" operation does not improve accuracy, it does minimize small discontinuities that would otherwise be present in the data. Such discontinuities are non-physical and can lead to problems when attempting model inversions. Next, the data are weighted to reflect the errors (as described below) and summed in the output buffer. The weighting factor, which includes the taper, are tracked in a separate buffer for each horizontal component. Once all the data have been summed, the data are normalized using the accumulated weights to compute the weighted average.

We used data with a variety of temporal baselines. With the tandem data we are able use 1, 35, and 36 day temporal baselines. The ERS-1 ice and commissioning phases yielded temporal baselines of 3, 6, and 9 days. The dominant noise sources in our data are atmospheric and other phase artifacts not related to interferometric decorrelation. Such artifacts should be largely independent of the temporal separation of images. As a result, we assume

the temporal baseline is inversely proportional to the relative phase errors, giving us an estimate of the relative variances of the phase errors.

Velocity estimates from a pair of overlapping ascending and descending interferograms may have different temporal baselines. Consequently, we estimated the phase variance for each interferogram separately and apply the appropriate rotation to derive the individual variance estimates for each component of velocity. The weighting factors for each component are then derived as one over the variance and used to weight the data as described above.

Comparison With GPS

The control for the velocity map, even with the bootstrapping described above, was based entirely on balance velocities and ice free points near the coast. We did not use the GPS velocities in any way to create the velocity map. Instead, we held these points back for use in validating our results. There were 12 GPS points that lie within the area that we mapped. These velocities are plotted as yellow vectors in Figure 1. For comparison we have included the corresponding interferometric estimates plotted as cyan vectors.

The RMS error for the interferometric estimates as given by Equation (1) is 5.0 m/yr. Table 1 gives the mean and RMS errors for the individual components and speed. At 4.7 m/yr the RMS error in the y direction is more than 2.5 times that in the x direction. The smaller error in the x component likely reflects the fact that many of the descending swaths, which are more sensitive to the x-component of velocity, have a temporal baseline of 35 or 36 days while none of the ascending data had a temporal baseline of more than 9 days.

	Mean	RMS
v_x	-0.9	1.7
v_y	1.1	4.7
$\|v\|$	0.6	3.3

Table 1: Mean and RMS difference between interferometric and GPS velocity estimates.

For the most part, the largest errors occurred among the 7 points that followed the NASA PARCA Greenland traverse. As indicated above, the control points in these faster moving regions are subject to larger errors, which may in part explain the larger errors.

It is interesting to note that two of the largest errors occur near the junction where the flow divides to feed Storstrømmen and Zacharie/Nioghalvfjerdsbrae. The dominant interferometric data in this region were collected with 6 day intervals in January and February 1994. With a relatively long temporal baseline of 6 days, the error should be relatively small in this region. Thus, we find it surprising that the largest errors were found at this location.

Storstrømmen surged from 1978-1984 (Reeh and Others, 1994). Mohr and others (1998) mapped the stagnant front of Storstrømmen interferometrically with ERS data acquired in 1995 and they concluded that the glacier is the process of returning to its pre-surge state. Thus, at least in its lower reaches, Storstrømmen is actively experiencing changes in its pattern of flow. Further inland, the NASA GPS velocity data were derived from displacements measured from surveyed pole locations in May of 1996 and 1997, roughly 2.5 years after the interferometric data were collected. Therefore, it is possible that the large difference for these two points during this period might be explained by changes in the relative discharge between post-surge Storstrømmen and Zacharie/Nioghalvfjerdsbrae.

Digital Elevation Model

In addition to velocity information, satellite radar interferometry can be used to estimate ice sheet elevation with resolution of 100-m or better (Joughin and Others, 1996a). In contrast, radar altimeters are limited to a much coarser resolution, usually several kilometers.

In addition to the direct glaciological applications, high resolution surface elevations are important for deriving interferometric estimates of velocity. In estimating motion there is first the direct effect of topography on interferometric phase, which must be separated from the motion signal. With reasonably short interferometric baselines (<100 m) radar altimetry derived DEMs are usually sufficiently accurate to allow a good separation of surface motion and topography. With existing SARs we are constrained to two look directions, yet there are three components of motion. With accurate surface slope information, under an assumption of surface parallel flow, the effects of vertical and horizontal motion can be separated to obtain an approximated estimate all three components from only two look directions (Joughin and others, 1998). Radar altimeters do not have sufficient resolution to capture much of the slope variability on an ice sheet. Improved estimates of ice motion can be made using a fine resolution DEM that captures more of the slope variability.

In theory, an ice sheet DEM can be created directly from the interferometric data, with other elevation information used only as a source of control. We began by creating a DEM from an 800-km long strip spanning the

length of the ice stream from sea-level to an elevation of greater than 3000 m. When we compared it with the altimetry data, we found long wavelength (100-km scale) errors with peak amplitudes of around 100 m. These errors correspond to phase errors of roughly one interferometric fringe (2π rad). We do not know the source of these errors; they could be the result of inhomogeneities in the troposphere or ionosphere, orbital variations of the spacecraft, drifting snow or other unknown causes. Similar errors were found in the other strips we processed. Regardless of the source of these errors, they are unacceptably large. We note that while such phase artifacts do affect the velocity estimates, we are able to mitigate their effects by using large temporal baselines or processing shorter segments of data where the baseline solution can partially correct longer wavelength errors.

Our initial DEMs revealed fine-scale structure (10-km scale) related to surface topography, whereas most of the errors seemed to occur over significantly longer length scales. Some of the DEMs exhibited streak-like errors (Joughin, 1996a) with 10 km scales along track and 100 km scale across track. In contrast the radar altimetry DEM had reasonable accuracy at the longer length scales, but much less short scale information. As a result, we decided to merge these data to retain the best aspects of both.

We blended the data using the wavelet decomposition routine provided by IDL (available from Research Systems, Inc.). The transform is based on a Daubechies wavelet filter (length=20). The transform decomposes the image into series of coefficients for orthogonal wavelet basis functions parameterized by length scale. Unlike a Fourier decomposition, the wavelet basis functions are localized in space. Using the altimetry DEM, we generated a second DEM in the same SAR-based coordinate system as the interferometric DEM. We performed the wavelet decomposition on both of these DEMs and substituted the shorter wavelength coefficients from the interferometric DEM for the corresponding coefficients in the altimetry DEM. We achieved the best results using a length-scale range for the interferometric data of 4-15 kilometers in the across-track direction and 4-30 kilometers in the along-track direction. We then computed the inverse transform for the combined coefficients to obtain a blended DEM. The blended swath DEMs were mosaicked to produce a DEM in polar stereographic coordinates. A shaded surface representation of the resulting DEM is shown in Figure 2.

The areas in Figure 2 with blended data correspond approximately to the regions with imagery in Figure 1. Outside these areas the data are derived from the altimetry based DEM. Surface topography with lengths scales of a few kilometers is far more evident in the blended data than in the nearby altimetry-based data. The addition of the interferometric data to the altimetry data appears to have produced a significant increase in resolution.

To assess the accuracy of the result, we have performed a comparison with a profile of laser altimetry data that runs down the length of the ice stream (see Figure 2). Assuming negligible error for the laser data (Krabill and other, 1995), the comparison gives an RMS error for the altimetry data of 16.0 m and a corresponding error of 13.0 m for the blended data. This modest improvement suggests there are still significant artifacts present in the interferometric data at shorter wavelengths.

More important than absolute accuracy for the elevation data used in producing the velocity estimates is the reduction in slope error. Along the laser profile, the altimetry DEM has an RMS slope error of 0.0082 while the slope error for the blended data is 0.0054. While this is not as good as we would have liked, the 34 percent reduction in slope error is a significant improvement for the separation of vertical and horizontal components of velocity.

Summary

We have demonstrated the ability to map the velocity field over an entire ice stream using satellite radar interferometry. Through the use of balance velocities, we have eliminated the need for *in situ* measurements for control. This approach should have wide application to other areas for velocity mapping. We have also shown modest improvements in resolution and height accuracy through the combination of interferometrically derived topography and radar altimetry data.

The continuous nature of the resulting data sets make the data ideal for constraining numerical models; we are in the process of finite element inversions of the data to improve constraints on bed and ice conditions.

Acknowledgments

I. Joughin performed his contribution to this work at the Jet Propulsion Laboratory, California Institute of Technology, under contract with NASA.

We thank S. Ekholm of the National Survey and Cadastre, Copenhagen Denmark for providing us with his DEM. We also wish to thank C. Werner of the Jet Propulsion Laboratory for providing us with a SAR processor for the raw signal data.

References

Bamber, J. L., S. Ekholm and W. B. Krabill. 1997. A digital elevation model of the Greenland Ice Sheet and validation with airborne laser altimeter data. Proceedings of the Third ERS Scientific Symposium, Volume 2., ESA Publication SP-414, Florence, Italy.

Bentley, C. 1987. Antarctic ice streams: a review," *J. Geophys. Res.*, **92**(B9), 8843-8858.

Ekholm, S. 1996. A full coverage, high-resolution, topographic model of Greenland, computed from a variety of digital elevation data. *J. Geophys. Res.*, **21**(B10), 961-972.

Fahnestock, M., R. Bindschadler, R. Kwok, and K. Jezek. 1993. Greenland Ice Sheet surface properties and ice dynamics from ERS-1 SAR imagery. *Science*, **262**, 1530-1534.

Goldstein, R. M., H. Engelhardt, B. Kamb, and R.M. Frolich. 1993. Satellite radar interferometry for monitoring ice sheet motion: application to an Antarctic ice stream. *Science*, **262**, 1525-1530.

MacAyeal, D. R., B. Bindschadler, T. Scambos. 1995. "Basal friction of Ice Stream E, West Antarctica," *J. Glaciol.*, 41(138), 247-262.

Joughin, I., D. Winebrenner, M. Fahnestock, R. Kwok, and W. Krabill. 1996a. Measurement of ice-sheet topography using satellite radar interferometry. *J. Glaciology,* **42**(140), 10-22.

Joughin, I., R. Kwok, and M. Fahnestock. 1996b. Estimation of ice-sheet motion using satellite radar interferometry. *J. Glaciology,* **42**(142), 564-575.

Joughin I., M. Fahnestock, S. Ekholm, and R. Kwok. 1997. Balance Velocities for the Greenland Ice Sheet, *Geophys. Res. Lett.,* **24**(23), 3045-48.

Joughin I., R. Kwok, and M. Fahnestock. 1998. Interferometric estimation of three-dimensional ice-flow using ascending and descending passes. *IEEE Trans. Geosci. Rem. Sen.*, **36**(1), 3045-3048.

Krabill W., R. Thomas, K. Jezek, K. Kuivinen, and S. Manizade. 1995. "Greenland ice-sheet thickness changes measured by laser altimetry," *Geophys. Res. Lett.*, **22** (17) 2341-2344.

Mohr, J.J., N. Reeh, S.N. Madsen. 1998. "Three-dimensional flow and surface elevation measured with radar interferometry," *Nature*, 391, 273-276.

Paterson, W. S. B., 1994. *The Physics of Glaciers.* 3rd Ed. Pergammon Press, Oxford.

Reeh, N., C. Bøggild, and H. Oerter. 1994. "Surge of Storstrømmen, a large outlet glacier from the inland ice of north-east Greenland," *Rapp. Grønlands geol. Unders.* **162,** 201-209.

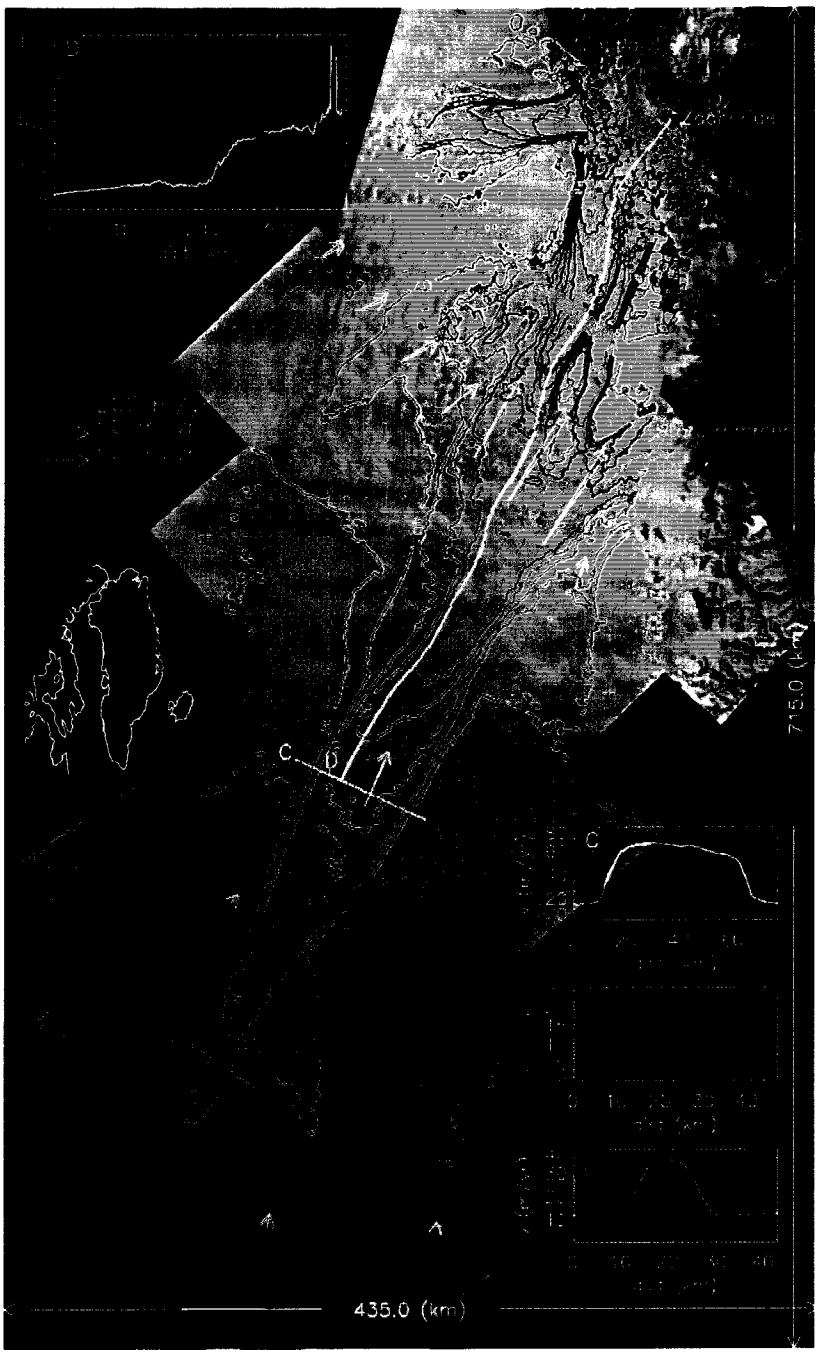

Figure 1. Velocity map for the Northeast Greenland Ice Stream. Green contours at 20 m/yr intervals are used for speed up to 80 m/yr while blue contours at 100 m/yr are used for higher speeds. Red arrows are used to show velocity. Speed is plotted along a set of four profiles (A,B,C, and D). Profiles A,B, and C are straight lines across the ice stream, while profile D corresponds to a flowline along the ice stream. Red '+' symbols mark the locations of GPS derived velocities. GPS velocities used for validation are illustrated with yellow vectors and cyan vectors are used for corresponding interferometric measurements. SAR imagery copyright ESA 1999.

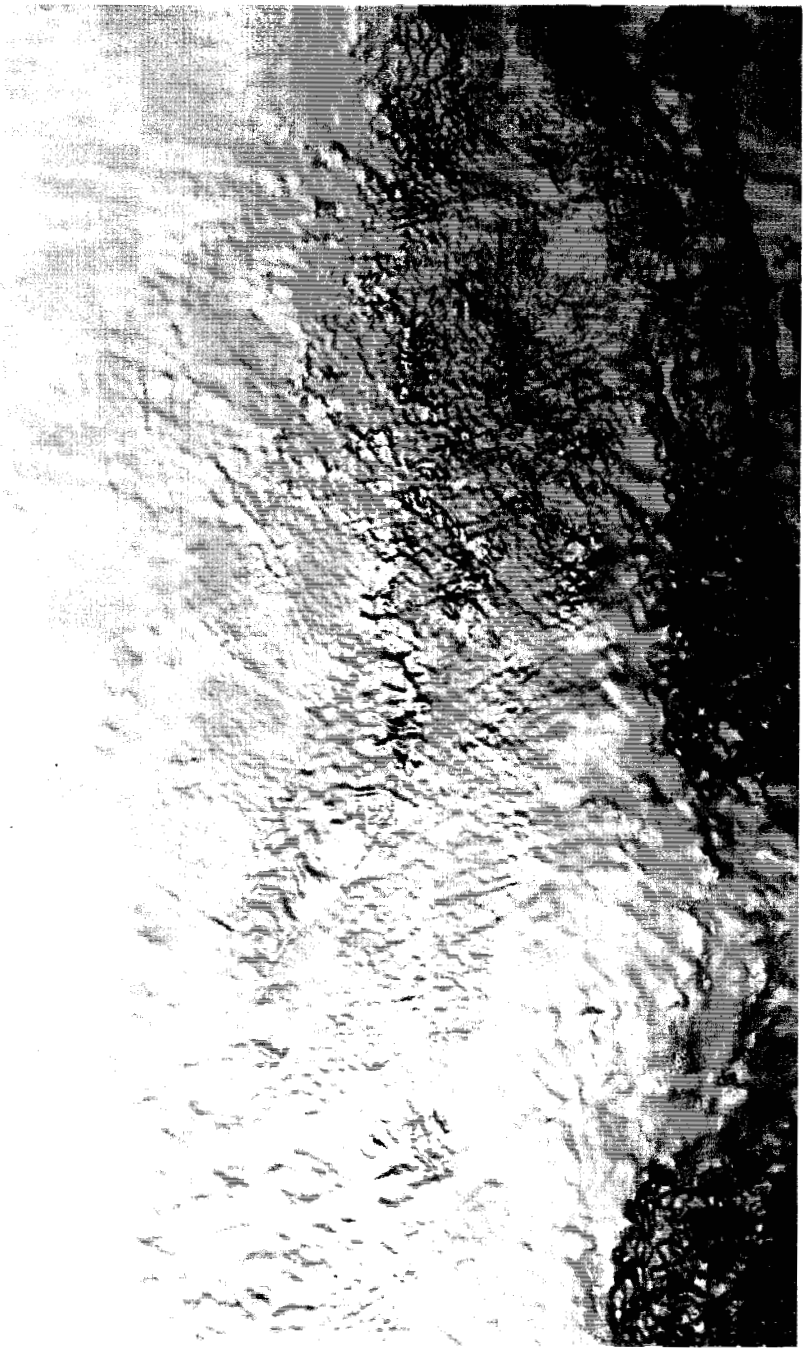

Figure 2. Shaded surface of DEM for the Northeast Greenland Ice Stream. The vantage point and light source are directly overhead. Where SAR data were available on the ice sheet, the DEM is a blend of interferometric and radar altimetry data. In other ice covered areas the data are primarily from radar altimetry. The ice free coastal data were photogrammetrically derived (Ekholm, 1996).